JOURNAL OF CHEMICAL INFORMATION AND MODELING

Article

pubs.acs.org/jcim

Structural Insights into Trapping and Dissociation of Small Molecules in K^+ Channels

Tobias Linder, Priyanka Saxena, Eugen Timin, Steffen Hering, and Anna Stary-Weinzinger*

Department for Pharmacology and Toxicology, University of Vienna, Althanstraße 14, 1090 Vienna, Austria

Supporting Information

ABSTRACT: K^+ channels play a critical role in numerous physiological and pathophysiological processes rendering them an attractive target for therapeutic intervention. However, the hERG K^+ channel poses a special challenge in drug discovery, since block of this channel by a plethora of diverse chemical entities can lead to long QT syndrome and sudden death. Of particular interest is the so-called trapping phenomenon, characterized by capture of a drug behind closed channel gates, which harbors an increased pro-arrhythmic risk. In this study we investigated the influence of trapped blockers on the gating dynamics and probed the state dependence of dissociation in K^+ channels by making use of the quaternary tetrabutylammonium. By applying essential dynamics simulations and two-electrode voltage clamp we obtained detailed insights into the dynamics of trapping in KcsA and hERG. Our simulations suggest that the trapped TBA influences the F656 flexibility during gate closure. Based on these findings, we provide a structural hypothesis for drug trapping. Further our simulations reveal the extent of gate opening necessary for drug dissociation.

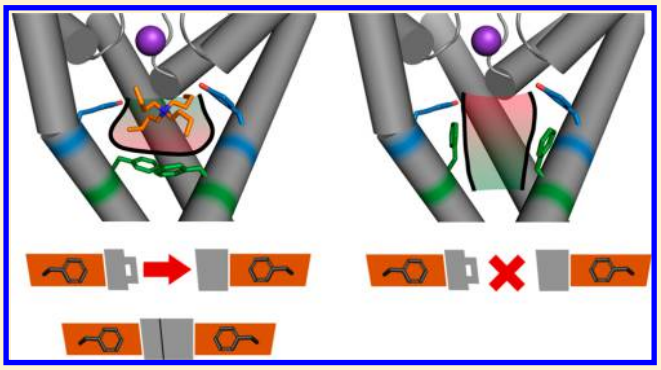

INTRODUCTION

Voltage gated K^+ channels play a critical role in numerous physiological and pathophysiological processes such as nerve and muscle excitation, sensory transduction, and cell proliferation. With a wide range of human diseases linked to voltage gated K^+ channels, so-called "channelopathies", they represent an attractive target for therapeutic intervention.[1] The human ether-à-go-go related gene (hERG) K^+ channel poses a special challenge in drug discovery, since it can be blocked by a plethora of structurally diverse drugs including antiarrhythmics, antihistamines, antipsychotics, and antibiotics.[2] This often unwanted inhibition can lead to acquired long QT syndrome (LQTS) and sudden cardiac death.[3,4] Consequently, several pharmaceuticals such as cisapride or terfenadine were withdrawn from the market. Further, reduced hERG channel function caused by inherited mutation leads to congenital LQTS. Recent research indicates that hERG channels are frequently overexpressed in certain human cancers and that long-term treatment with blockers could have therapeutic potential in cancer treatment.[5,6] Thus, pharmacological intervention could potentially be useful for cancer treatment and clinical management of LQTS.

Great efforts have been directed toward a better understanding of the molecular and structural mechanisms of hERG channel gating and block. Substantial progress has been made by identifying the amino acids essential for drug block. They include T623, S624, and V625, from the pore helix, and residues G648, Y652, and F656, located on the TM2 segments.[7−20] However, a key unresolved question in hERG channel block is how drug dissociation is influenced by channel closure. There is evidence that hERG channel blockers can be trapped in the inner cavity of the closed channel.[14,15,18,20−24] The importance of this phenomenon is emphasized by a recent study highlighting a connection between pro-arrhythmic risk and trapping.[25]

The trapping phenomenon in K^+ channels was first described for quaternary ammonium (QA) blockers by Armstrong in 1971.[26] Since then, QA compounds have been widely used as structural probes to identify the binding side of ion channel blockers,[27−30] to investigate gating processes,[31,32] and to shed light on the structure of ion channels.[33−36]

Herein, we set out to investigate the influence of trapped blockers on the gating dynamics and probe the state dependence of dissociation in K^+ channels by making use of the QA blocker tetrabutylammonium (TBA). The crystal structure complex of the prototypical K^+ channel KcsA with a TBA bound in the closed channel pore[37,38] provides an excellent starting point to analyze trapping dynamics and drug dissociation pathways in K^+ channels. We utilized essential dynamics (ED) simulations and two-electrode voltage clamp to obtain detailed insights into the dynamics of trapping in KcsA and hERG. Further, free energy calculations were performed to examine state dependent dissociation of a trapped channel blocker.

Received: June 16, 2014
Published: October 9, 2014

METHODS

MD Simulations. The crystal structure (pdb identifier: 2HVK), comprising of the closed KcsA channel from residue 22 to 124 and the cocrystallized trapped TBA,[38] was used as a starting point for MD simulations. The open (pdb identifier: 3f7v) and the intermediate (pdb identifier: 3fb6) channel states were obtained from Cuello et al.[39] Due to crystallization of shorter fragments in the latter two structures, the missing amino acids at the N- and C-termini below the bundle crossing gate were added using Discovery Studio 3.5 (Accelrys Software Inc., San Diego, CA, USA) to obtain channel states of the same length. In addition, the introduced cysteine at position 90 in the crystal structures was mutated back to the WT leucine. TBA was added to the open and intermediate channels by placing it in the cavity according to the closed channel binding site. Further, TBA was docked to the open hERG homology model[40] using FlexX which is part of the LeadIT software package version 2.0.1 (BioSolveIT, Sankt Augustin, Germany). The sphere center of the binding site was placed in the middle of the cavity, and the radius was set to 10 Å. General amber force field parameters[41] for TBA were generated by making use of Gaussian09[42] and antechamber[43] which is part of the amber package.[44] Protein−ligand complexes were embedded in an equilibrated palmitoyloleoylphosphatidylcholine (POPC) membrane consisting of 256 lipids using the g_membed tool.[45] K^+ ions were placed in the selectivity filter (SF) at sites S0, S2, and S4, and water was added at S1 and S3.[46] The system was neutralized by randomly adding Cl^- within the solvent. All simulations were carried out using the MD simulation software Gromacs v.4.5.4.[47] The amber99sb force field[48] and the TIP3P water model[49] were employed. Lipid parameters were taken from Berger et al.[50] The cutoff for Lennard-Jones interactions was set to 1.0 nm, and parameters were corrected for monovalent ions.[51] Electrostatic interactions were calculated with a cutoff of 1.0 nm, and long-range electrostatic interactions were treated by the particle-mesh Ewald method at every step.[52] The LINCS algorithm[53] was used to constrain bonds, allowing for an integration step of 2 fs. The Nose-Hoover thermostat[54,55] was used keeping the simulation temperature constant at 310 K. Coupling groups were defined as the protein−ligand complex, lipids, and solvent with a time constant of 0.2 ps. The Parrinello−Rahman barostat algorithm[56] with a coupling constant of 1 ps was used for a constant pressure of 1 bar. Prior to simulation, 1000 conjugate gradient energy-minimization steps and a 5 ns equilibration run by restraining the protein−ligand complex by a force constant of 1000 kJ/mol/nm^2 were performed. Subsequent free MD simulations were carried out for 20 ns in KcsA and for 100 ns in hERG.

Essential Dynamics Simulations. The ED technique was employed as described previously.[57] Briefly, an eigenvector representing the transition between open and closed channel state was obtained from principal component analysis. For this analysis, the backbone of the helices between the two states was compared. Fixed increment linear expansion was set to $-1.69e^{-6}$ nm per simulation step (2 fs). Twenty closing ED simulations, lasting for 20 ns each, were performed in the absence and presence of TBA for KcsA and hERG channels, respectively.

Force Probe MD Simulations and Umbrella Sampling. To probe different dissociation pathways of TBA, a harmonic potential with a force constant of 1000 kJ/mol/nm^2 was applied on TBA. The compound was pulled for 20 ns with a rate of 0.00025 nm/ps along the z-axis to investigate dissociation through the activation gate. The first turn of the extracellular side of the P-helix was restrained with a force constant of 1000 kJ/mol/nm^2 during pulling to prohibit movement of the protein. For dissociation simulations of the open KcsA and hERG channels, ions were restrained with a force constant of 10000 kJ/mol/nm^2 to prevent ion migration through the gate and minimize the ion influence on drug dissociation. In case of dissociation experiments on KcsA, 95, 99, and 56 snapshots from closed, intermediate, and open state simulations were extracted, respectively, and subject to 20 ns umbrella sampling with force constants of either 1000 or 10000 kJ/mol/nm^2. For hERG dissociation, 57 snapshots from open simulations were obtained and used for umbrella sampling accordingly (histograms of umbrella sampling simulations are shown in the Supporting Information). The first 10 ns of each window were discarded for equilibration. The potential of mean force and the statistical errors were estimated by the g_wham tool and the integrated bootstrap analysis method using 100 bootstraps.[58]

Experimental Procedure. cDNAs of hERG (accession number NP000229) were kindly provided by Prof. Sanguinetti (University of Utah, UT, USA). Synthesis of capped runoff complementary ribonucleic acid (cRNA) transcripts from linearized cDNA (cDNA) templates and injection of cRNA were performed as described in detail by Sanguinetti et al.[59] Oocytes from the South African clawed frog, *Xenopus laevis* (NASCO, Fort Atkinson, WI, USA), were prepared as follows: After 15 min exposure of female *Xenopus laevis* to the anesthetic (0.2% solution of MS-222; the methanesulfonate salt of 3-aminobenzoic acid ethyl ester; Sigma), parts of the ovary tissue were surgically removed. Defolliculation was achieved by enzymatical treatment with 2 mg/mL collagenase type 1A (Sigma) and mechanical removal of follicular layer using forceps. Stage V−VI oocytes were selected and injected with the WT and mutant hERG-encoding cRNA. Injected oocytes were stored at 18 °C in ND96 bath solution (96 mM sodium chloride, 2 mM potassium chloride, 1 mM magnesium chloride, 5 mM HEPES, 1.8 mM $CaCl_2$; pH 7.5, titrated with NaOH) containing 1% penicillin-streptomycin solution. All chemicals used were purchased from Sigma-Aldrich Chemie GmbH, Taufkirchen, Germany.

Currents through hERG channels were studied 1 to 4 days after microinjection of the cRNA using the two-microelectrode voltage clamp technique. ND96 was used as extracellular recording solution. Voltage-recording and current-injecting microelectrodes were filled with 3 M KCl and had resistances between 0.3 and 2 MΩ. Endogenous currents (estimated in oocytes injected with DEPC water) did not exceed 0.15 μA. Currents >5 μA were discarded to minimize voltage clamp errors. Ionic currents were recorded with a Turbo Tec 03X Amplifier (npi electronic, GmbH, Tamm, Germany) and digitized with a Digidata 1322A (Axon Instruments Inc., Union City, CA, USA). The pClamp software package version 9.2 (Axon Instruments Inc.) was used for data acquisition. Microcal Origin 7.0 was employed for analysis and curve fitting.

A precondition for all measurements was the achievement of stable peak current amplitudes over periods of 10 min after an initial run-up period. A frequency of 0.3 Hz was used for all voltage clamp experiments. Drugs were applied by means of a perfusion system enabling solution exchange within 100 ms.[60] The oocytes were kept for 5 min at a holding potential of −100 mV to equilibrate drug diffusion. The tail current was measured

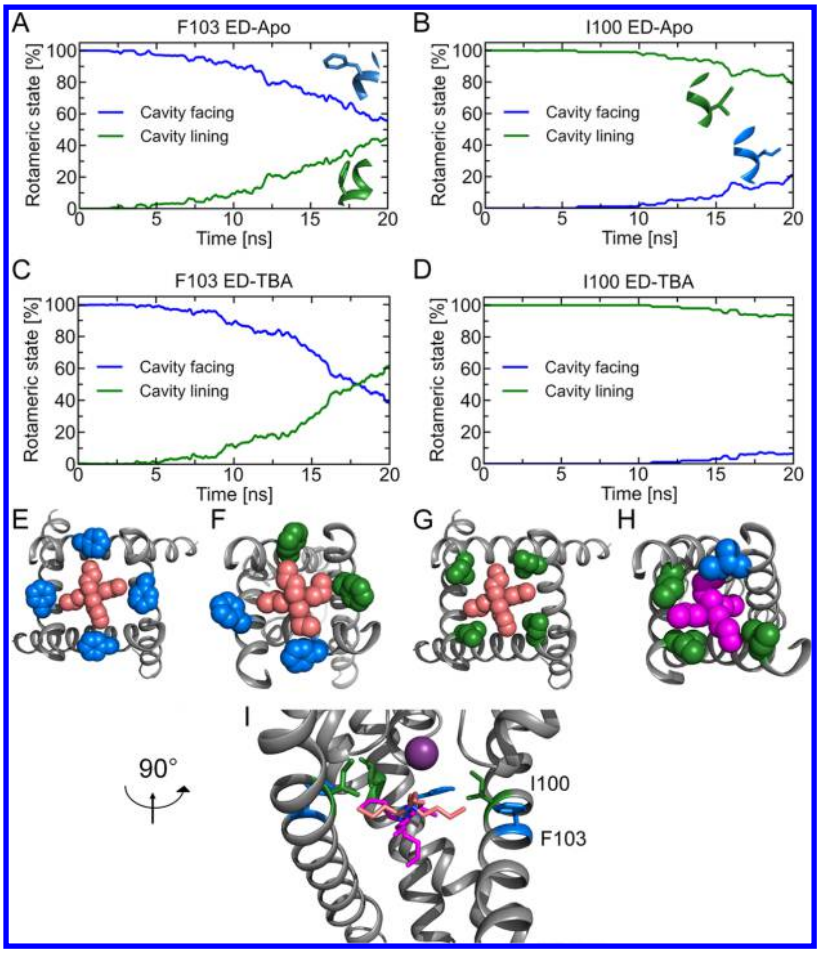

Figure 1. Rotameric states of F103 and I100 during KcsA gate closure. Conformational changes of F103 (A and C) and I100 (B and D) in the absence (A and B) and presence (C and D) of TBA during gating. The cavity facing (χ_1 angle < −123°) and cavity lining (χ_1 angle > −123°) states are shown as blue and green lines, respectively. Panels E and F show the rotameric states of F103 as spheres at the beginning and end of gate closure in top view, respectively. In panels G and H, I100 is shown as spheres accordingly. Panel I represents the xy-plane (pink sticks) and tilted (magenta sticks) orientation of TBA in the side view. For clarity, only three SUs are shown in gray. The K^+ ion in the SF is represented as a violet sphere. The color code of the amino acids corresponds to the rotameric states.

at −50 mV, after a step to +20 mV. Use-dependent hERG channel block was estimated as peak tail current inhibition. Data are presented as means ± s.e. from at least four oocytes from ≥2 batches; statistical significance of differences was defined as $P < 0.0001$ in Student's unpaired *t*-test. The studied compound TBA was obtained from Sigma and was dissolved in ND96 extracellular recording solution to prepare a 1 M stock on the day of experiments. Drug stock solution was further diluted to the required concentration.

RESULTS

TBA Trapping Simulations in KcsA. Using MD simulations, we have previously identified key residues in KcsA essential for gating.[57] In particular, we found that the TBA binding determinant F103 changes its rotameric state during channel gating. Thus, to investigate the influence of TBA on conformational changes upon channel closure, 20 ED simulations with and without TBA present in the cavity were performed which enable simulating channel closure on the ns time scale.[57] Each closing simulation was conducted for 20 ns. ED is a free MD simulation method, with all coordinates equilibrating, except for one coordinate, which is derived from a linear interpolation between the open and closed helix backbone structures and is biased to drive gating. All other degrees of freedom are explicitly allowed to relax continuously, enabling investigation of side chain conformational changes during drug trapping.

Specifically, the χ_1 angle of the binding site forming F103 and I100 was monitored and separated into the two possible rotameric states, namely cavity lining (χ_1 angle > −123°) and cavity facing (χ_1 angle < −123°) state. Subsequently, the percentage of the two states was calculated for each time step and plotted over time (Figure 1). In the absence of TBA (Figure 1A), nearly equal distribution between the two states was observed at the end of gate closure for F103, which is in good agreement with our previous work.[57] In the presence of TBA, only a slightly faster rotameric switch from cavity facing to the cavity lining was observed over time leading to a preference of the cavity lining conformation at the end of gate closure (Figure 1C). The second important binding determinant, I100, displayed high stability during gating. Only rare changes from the cavity lining to the cavity facing conformation were detected with negligible impact by the bound TBA (Figure 1B and D).

Crystallographic data in combination with MD simulations revealed that TBA can adopt two different orientations in the KcsA binding site linked to the ion configuration in the SF.[37]

dx.doi.org/10.1021/ci500353r | J. Chem. Inf. Model. 2014, 54, 3218−3228

Throughout gate closure, TBA remained in the high affinity binding site formed by F103 and I100 (Figure 1E−H). TBA is either in an xy-plane orientation which is parallel to the membrane plane and is centered on the channel symmetry axis. In this orientation, the butyl side chains project into the grooves formed by I100 and F103. Alternatively, TBA adopts a tilted, vertical orientation which is indicated by an off-axis center of TBA (Figure 1I). In the gating simulations, sampling of the xy-plane and the tilted orientation was observed independent of the ion configuration in the SF. No specific pattern between F103 switch and TBA orientation was found indicating that F103 can either face or line the cavity and still allow both TBA orientations. In the rare observations where I100 faced the cavity, spatial displacement led to the tilted orientation of TBA (Figure 1H).

TBA primarily exists in two conformations. The energetically more favorable D_{2d} conformation exhibits a cross-shaped structure with all four butyl chains in a planar arrangement, while the S_4 conformation exhibits the shape of an inverted tetrahedron. Quantum-mechanical calculations of the QA analogue tetraethylammonium (TEA) have shown that the D_{2d} state is separated from the S_4 conformation by energy barriers of around 10 kcal/mol and a total energy difference of around 1 kcal/mol.[61] The energy difference between the two states is similar for TBA.[62] Throughout the closing process, TBA stayed in the D_{2d} conformation (see supplemental Figure S1), which is in good agreement with previous TBA simulations in the closed channel.[37] Only rare transitions to the S_4 conformation were observed. This suggests that TBA does not have to change its conformation in order to allow rotation of the F103 side chain. In addition, this observation indicates that the TBA conformation is independent of the rotameric state of F103. Taken together, our data suggests that TBA does not interfere with side chain rearrangements necessary for gating in KcsA.

Experimental Characterization of hERG Channel Block by TBA. Despite the crucial role of drug trapping in hERG channels[25] the structural interplay between drug and channel during closure are not well understood. Again, we resorted to the well-studied model drug TBA to investigate trapping in hERG. It was previously shown by Choi et al.,[63] that externally applied TBA presumably blocks hERG from the intracellular side by permeating through the cell membrane in CHO cells. However, the characteristics of TBA block were not investigated in detail. Therefore, we set out to test whether TBA is trapped in hERG channels expressed in *Xenopus* oocytes by using the two-electrode voltage-clamp technique.

hERG channels were activated and subsequently inactivated by 300 ms depolarization to +20 mV (Figure 2A). Upon repolarization to −50 mV, channels undergo rapid recovery from inactivation inducing a large tail current. In order to analyze state-dependent block, currents were measured in the absence of TBA (control, Figure 2A) and after preincubation for 330 s with 20 mM TBA while holding at −100 mV. Subsequently, 0.3 Hz pulse trains were applied until steady state block was reached. The ratio between tail current amplitude in the presence of TBA and tail current amplitude in the control solution was taken as a measure of block. Channel block developed in a "use-dependent" manner. The first current after the 330 s equilibrium in TBA displayed a pronounced decay during the 300 ms prepulse to +20 mV (Figure 2A, p1) with a significant tail current inhibition. Prepulse and tail currents were further inhibited during the 0.3 Hz pulse train. The steady

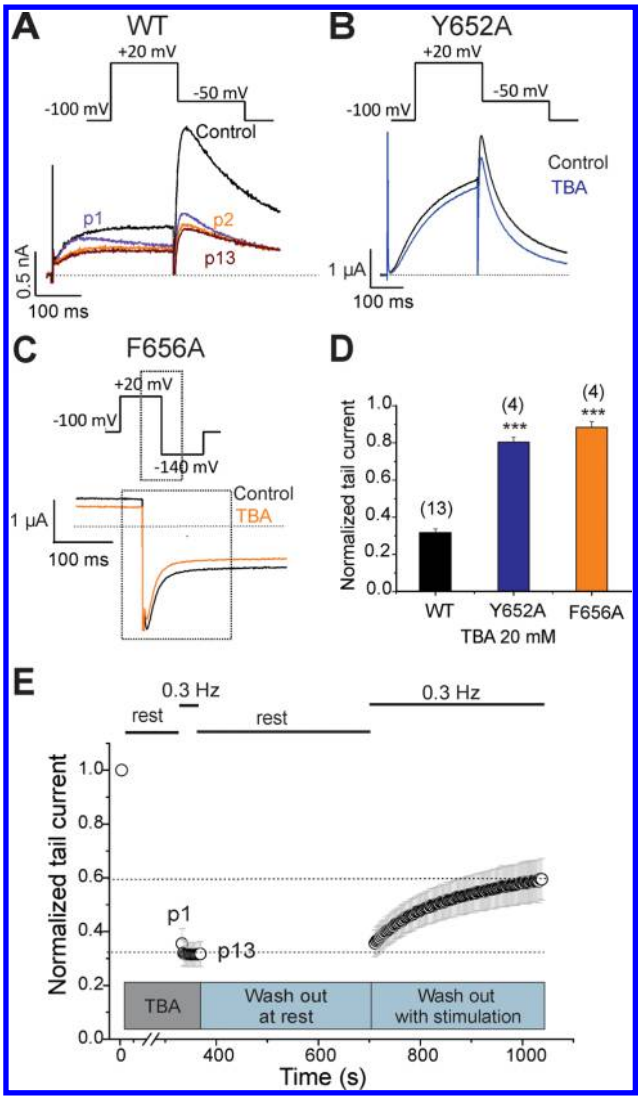

Figure 2. WT and mutant hERG channel inhibition by TBA. A) Superimposed current traces in the absence of TBA (control, black) and after a 330 s preincubation period in 20 mM TBA (p1, magenta). Steady state block occurred within the first 2 pulses (p2, orange and p13, brown). The voltage protocol is shown on top of the current traces. B and C) Representative current traces and corresponding voltage protocols for current measurements of mutants Y652A and F656A in the absence (Control, black trace) and presence of 20 mM TBA (blue and orange trace, respectively). Tail currents of F656A were recorded at −140 mV. D) Normalized peak tail currents of WT, Y652A, and F656A channels after steady state block by 20 mM TBA (n = 4−13, error bars, ± SEM; unpaired t-test, $P < 0.0001$). E) State dependent recovery of hERG channels from TBA block. Peak tail currents were normalized to control currents and plotted against time. After 330 s incubation of WT hERG channels with 20 mM TBA, steady state block was reached within the first 2 pulses of a 0.3 Hz pulse train (p1−p13). During the following 330 s wash period, channels were kept closed at resting potential of −100 mV. Recovery from block at rest was probed by subsequent pulsing at 0.3 Hz.

state block was achieved rapidly within the first 2 pulses (Figure 2A; p2, p13). The development of block during channel activation at +20 mV suggests that TBA blocks hERG channels in an open channel conformation. Twenty mM TBA blocked hERG channels by 68.3 ± 2.0% (Figure 2D).

To identify amino acids essential for TBA block, we performed alanine mutation studies on Y652 and F656 which

dx.doi.org/10.1021/ci500353r | J. Chem. Inf. Model. 2014, 54, 3218−3228

have been shown to play a key role for binding of different chemical entities.[16] The WT channel voltage protocol was utilized for Y652A, while tail currents were measured at −140 mV for F656A as reported by Witchel et al.[15] Y652A and F656A significantly reduced channel inhibition to 19.6 ± 2.7% and 11.7 ± 3.2%, respectively (Figure 2B−D). This is in line with data shown in Figure 2A suggesting that TBA accesses a binding site inside the cavity comprising of the two prominent aromatic residues.

Next, we probed if TBA is trapped inside the hERG cavity as suggested for KcsA.[30,37,38] The hallmark of drug trapping is an ultraslow recovery or lack of recovery at rest.[18,22−24] Recovery of hERG from TBA block during a 0.3 Hz train was monitored after a 330 s period at holding potential of −100 mV where the channels are in a closed resting state. During this rest period, the oocytes were perfused with TBA-free solution (Figure 2E). The first current amplitudes after this rest period recovered from block only by 5 ± 1.1% indicating that TBA is trapped in the closed channel conformation. Subsequent frequent opening of the channel during continuous stimulation at 0.3 Hz induced monoexponential recovery from TBA block to 41.3 ± 8.3% in 330 s (Figure 2E) suggesting that trapped TBA leaves the channel during activation when the channels are in an open conformation.

Structural Insights of TBA Block in hERG. To further explore TBA hERG channel interactions, we docked TBA into the hERG cavity using the program FlexX and the open hERG homology model.[40] In the docking simulations, the tilted orientation is favored over the xy-plane orientation thereby maximizing hydrophobic interactions of TBA with Y652 and F656 (Figure 3A and B). In a subsequent 100 ns MD simulation starting from the best ranked docking pose, TBA sampled both planar and tilted orientations equally, closely interacting with the two aromatic amino acids Y652 and F656. In Figure 3C, the shortest distances between a TBA side chain and the aromatic rings of Y652 and F656 are plotted over time. Distances between 4 and 6 Å indicate that TBA side chains favorably interact with the aromatic amino acids. Further, the central ammonium group of TBA is positioned in the center of the pore, near the K^+ binding site, suggesting that the helix dipole charges from the pore helices contribute to binding.

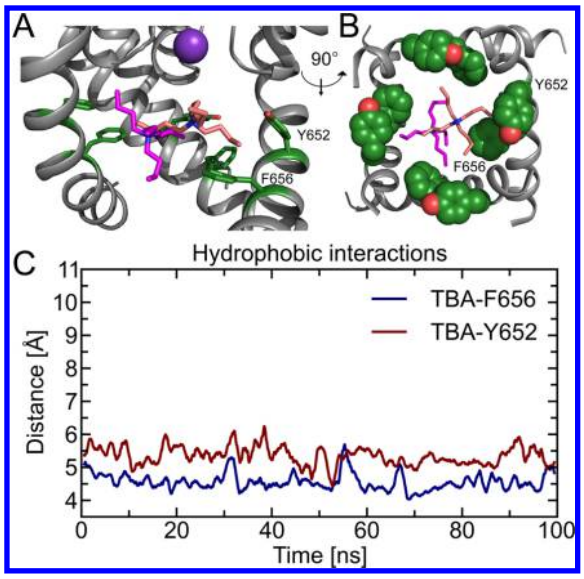

Figure 3. Orientation of TBA in hERG and distances between TBA side chains and Y652 and F656. A) TBA in the xy-plane (pink sticks) and tilted (magenta sticks) orientation in side view. For clarity, only three SUs are shown in gray. The K^+ ion in the SF is represented as a violet sphere. Y652 and F656 are shown as green sticks. B) Top view of TBA in the xy-plane (pink sticks) and tilted (magenta sticks) orientation. Y652 and F656 in the cavity facing state are shown as green spheres. C) Distances between TBA side chains and Y652 and F656. The distance between the three outermost carbon atoms of each butyl side chain and the aromatic rings was calculated. The closest distance at each time step is plotted.

Measured distances between the quaternary nitrogen of TBA and Y652 and F656 were always above 5.5 Å in our simulation. At such distances the potential energies of cation-pi interactions become insignificant.[64] Further, interactions between the aromatic rings and the H atoms on the carbons adjacent to the protonated nitrogen, as described by Imai et al.,[74] were above 4.5 Å. Therefore, it is unlikely that cation-pi stacking contributes to binding. Throughout the simulations TBA remained in the energetically favorable D_{2d} conformation.

Dynamics of TBA Trapping in hERG. To investigate possible conformational changes during hERG gating, we performed 20 ED simulations in the absence and presence of TBA. The apo simulations revealed that the conformation of Y652 remains in the cavity facing orientation, independent of channel state (Figure 4A). In contrast the rotameric state of the second aromatic amino acid forming the binding site, F656 changed dramatically during gate closure. While preferably in the cavity facing conformation in the open channel state, F656 switched rapidly to the cavity lining conformation in the apo simulations, reaching equal distribution between the two states after 8 ns (Figure 4B). Interestingly, a third, rare rotameric state of F656 was observed during gating. F656 can rotate to a state orthogonally to the S6 helix since two adjacent S6 helices approach each other during closing and therefore decrease the space in this region. These findings show that Y652 remains rigid during gating while F656 undergoes gating specific rotameric changes.

Next, we probed the influence of TBA on gating dependent rearrangements of binding residues. We observed no significant differences for Y652 (Figure 4C). However, TBA clearly influenced the dynamics of F656 during trapping. Figure 4D illustrates that TBA slows the transition from the cavity facing to the cavity lining conformation. In simulations without the blocker, equal distribution was reached after 8 ns, while in the presence of TBA, 15 ns were necessary. This suggests that the trapped TBA stabilizes the F656 conformation in cavity facing orientation.

As observed in KcsA, TBA remains in the D_{2d} conformation with rare observations of the S_4 state during hERG channel closure (supplemental Figure S2). Due to the larger cavity, TBA can adopt the tilted as well as the xy-plane orientation (Figure 4E and F).

State Dependence of TBA Dissociation. While it was shown that dissociation of trapped compounds is explicitly linked to an open gate, the extent of gate opening necessary for dissociation remains elusive. Crystal structures of KcsA in closed, intermediate, and open states[39,65] and a cocrystallized TBA[37,38] provide an ideal set of structural information to probe state dependent dissociation. The closed channel with TBA, crystallized by Yohannan et al.,[38] served as a starting point. TBA was placed to the same binding site in the intermediate and open channel state,[39] and all systems were subject to 20 ns free MD simulation to allow equilibration of TBA orientation.

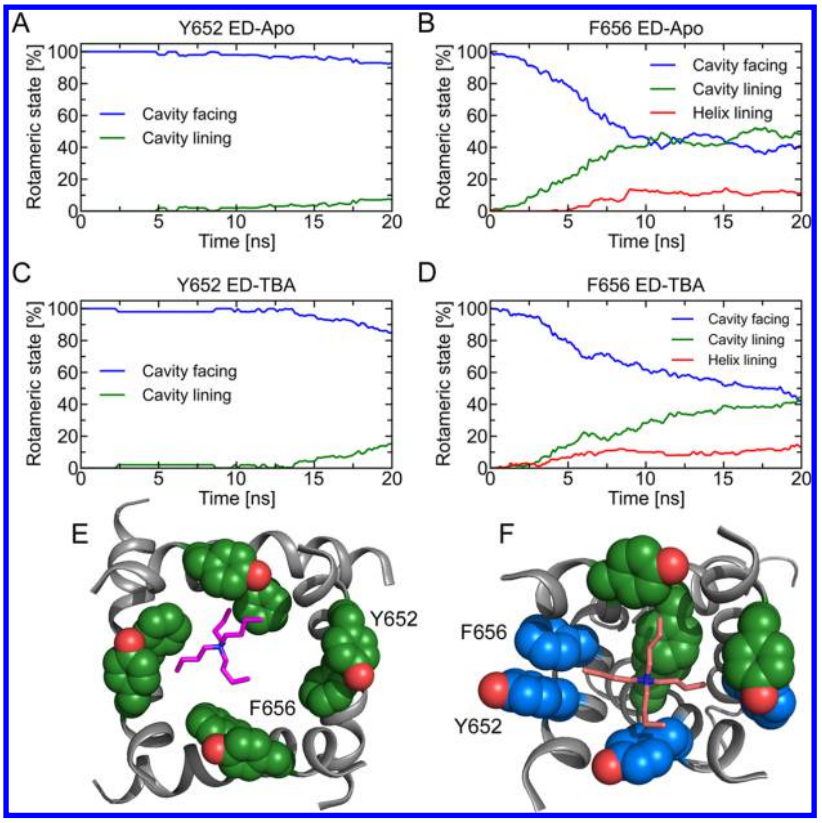

Figure 4. Rotameric states of Y652 and F656 during hERG gate closure. Conformational changes of Y652 (A and C) and F656 (B and D) in the absence (A and B) and presence (C and D) of TBA during gating. Cavity facing (blue line) and cavity lining (green line) states identified for KcsA also apply for hERG. For F656, an additional helix lining state (χ1 angle in the range of 80°, red line) was observed. E and F) Rotameric states of Y652 and F656 as spheres at the beginning and end of gate closure in top view, respectively. TBA is represented as sticks and colored magenta and pink in the tilted and xy-plane orientation, respectively. Y652 and F656 are colored according to their rotameric states.

TBA remained in the xy-plane orientation as seen in the crystal structures.[37,38] Subsequently, force probe MD simulations were used to pull the compound along the channel axis through the gate region. Free energy calculations of the dissociation pathway by umbrella sampling provide qualitative insights into the probability of TBA dissociation from specific channel states. In the closed KcsA channel, TBA is tightly packed in the cavity formed by F103 and I100 as well as by T107 where the pore becomes constricted (see Figure 5B and C). The small energy well in the cavity and the large energy increase along the *z*-axis indicate that the cavity space in the closed state is very limited (Figure 5A). Squeezing TBA through the closed gate (Figure 5D−G) led to a total energy barrier of 50 kcal/mol rendering spontaneous dissociation through the closed gate very unlikely. Even at the membrane solvent interface region the barrier remains high, due to unfavorable interactions of TBA with the pH sensing residues of KcsA (Figure 5H). During the force probe simulation, TBA adopted and remained in the S_4 conformation. This suggests that part of the applied energy, contributing to the energy barrier, is used to change the TBA conformation. In addition, up to 1 kcal/mol might be stored in the S_4 conformation.

Next, TBA was pulled through the intermediate channel gate (gate diameter of 8 Å). The opening of the gate increased the cavity size leading to a broader energy well of TBA in the binding site. However, an energy barrier of 40 kcal/mol was calculated for TBA dissociation (Figure 6A−G). Again, TBA adopted the S_4 conformation during dissociation and stayed in that conformation. Similar to dissociation from the closed state the barrier remains high, when reaching the membrane solvent interface region. As can be seen in Figure 6G, in the region of 4.2 to 4.6 nm on the *z*-axis, TBA passes the pH sensing residues of KcsA.

In the open KcsA channel, the cavity (gate diameter of 14 Å) is directly accessible to the solvent. The force probe MD simulations revealed that TBA, due to its hydrophobic nature, moves along the TM2 and TM1 helices before it gets fully hydrated in the intracellular compartment. Free energy calculations showed that the open gate does not cause an energy barrier for TBA dissociation (Figure 7A). The increase in energy during dissociation is mainly caused by TBA leaving its high affinity binding site between 2 and 2.5 nm on the *z*-axis (Figure 7A, B−D). A total energy difference of 8 kcal/mol between the bound and the solvated TBA was measured. Throughout the dissociation simulation, TBA remained in the D_{2d} conformation further indicating that the gate is wide enough to allow dissociation of a planar TBA which has a diameter of 12 Å (Figure 7B−F).

TBA Dissociation from the Open hERG. To explore dissociation of TBA from the hERG channel we applied force probe simulations and umbrella sampling, as described above for KcsA. TBA dissociation was only probed from the fully open hERG state since free energy calculations on KcsA suggest that dissociation solely occurs from an open channel state.

For hERG dissociation, a total energy difference of 6 kcal/mol was measured (Figure 8A−C). At position 2.2 to 2.4 nm on the *z*-axis, an interacting F656 switched from the cavity facing to the cavity lining state, thereby allowing easier passage

dx.doi.org/10.1021/ci500353r | J. Chem. Inf. Model. 2014, 54, 3218−3228

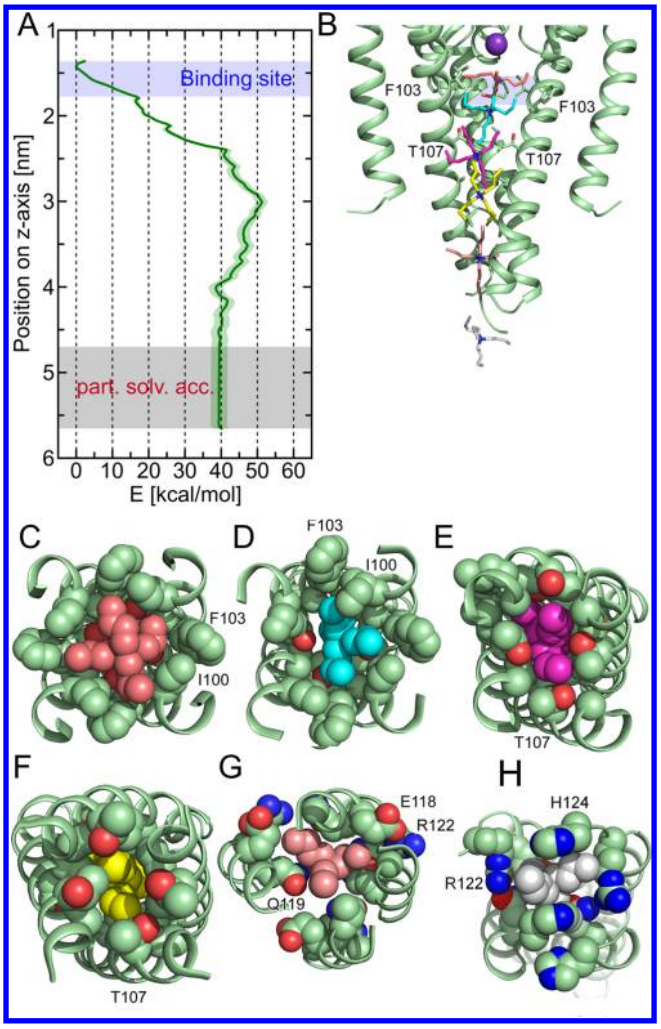

Figure 5. A) Free energy profile of TBA dissociation from the closed KcsA channel. The blue and gray shades depict the partially solvent accessible membrane water interface (part. solv. acc.), respectively. Statistical error is shown as green shade. B) TBA structures, represented as sticks, show the dissociation pathway through the gate. For clarity, only three SUs are shown in green. Interacting amino acids are depicted as green sticks. The K^+ ion in the SF is represented as a violet sphere. TBA structures in panel B and C−H correspond to positions 1.45 nm (pink, C), 1.84 nm (cyan, D), 2.45 nm (magenta, E), 3.0 nm (yellow, F), 4.0 nm (light pink, G), and 5.3 nm (gray, H) on the *z*-axis. C−G) Top view of TBA and interacting amino acids during dissociation. H) Bottom view of TBA with interacting charged residues from the pH sensor. TBA is colored according to its position, and amino acids are shown as green spheres with one SU labeled.

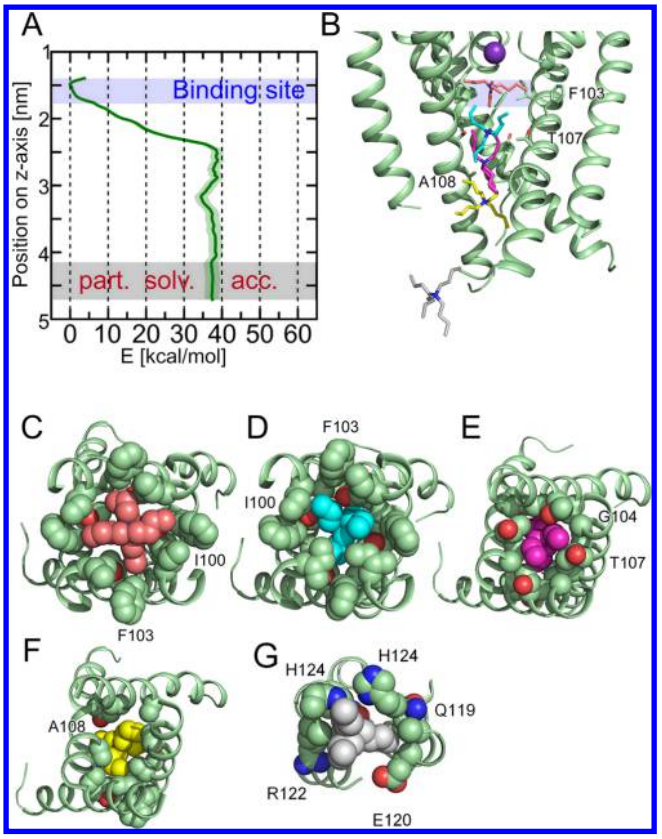

Figure 6. A) Free energy profile of TBA dissociation from the intermediate KcsA channel. The blue and gray shades depict the high affinity binding site and the partially solvent accessible membrane water interface (part. solv. acc.), respectively. Statistical error is shown as green shade. B) TBA structures, represented as sticks, show the dissociation pathway through the gate. For clarity, only three SUs are shown in green. Interacting amino acids are depicted as green sticks. The K^+ ion in the SF is represented as a violet sphere. TBA structures in panels B and C−F correspond to positions 1.5 nm (pink, C), 2.1 nm (cyan, D), 2.5 nm (magenta, E), 3.2 nm (yellow, F), and 4.4 nm on the *z*-axis (gray, G). C−F) Top view of TBA and interacting amino acids during dissociation. TBA is colored according to its position, and amino acids are shown as green spheres with one SU labeled. G) Bottom view of TBA and interacting charged residues from the pH sensor.

of TBA through the channel gate and causing an energy plateau phase. The subsequent energy barrier from 2.5 to 3 nm is caused by the first exposure of TBA to the solvent after the F656 passage (Figure 8D and E). At 3 nm on the *z*-axis (Figure 8E), TBA packs to two adjacent TM2 helices before it gets fully hydrated shown by an energy increase to 6 kcal/mol. Throughout the dissociation simulation, TBA remained in the D_{2d} conformation.

DISCUSSION

In this study we addressed two important questions concerning drug trapping in K^+ channels. First, do trapped drugs influence gating? Second, is a fully open gate required for drug dissociation? To answer the first question, we performed MD simulations with the prototypical K^+ channel KcsA and a model of the hERG K^+ channel. Closing ED simulations with TBA in KcsA and hERG revealed that the drug influences structural rearrangements in hERG but not in KcsA. This is in agreement with crystal structures of TBA trapped in KcsA by Faraldo-Gómez et al.[37] and Yohannan et al.[38] indicating a negligible effect of drug block on the channel structure.

In hERG, experimental characterization of TBA block was lacking so far. Thus, we first investigated the mechanism of TBA hERG interactions in detail. Open/inactivated channel dependence of block of TBA was indicated by fast current decrease upon channel activation (Figure 2A). This finding is in line with the well described state dependence of drug block in hERG.[66,67] Alanine mutations of Y652 and F656 revealed that both residues significantly reduce the potency of TBA (Figure 2D) indicating that this compound binds to the cavity as has been shown for a multitude of other hERG blockers.[7−10,12−14,18−20]

dx.doi.org/10.1021/ci500353r | J. Chem. Inf. Model. 2014, 54, 3218−3228

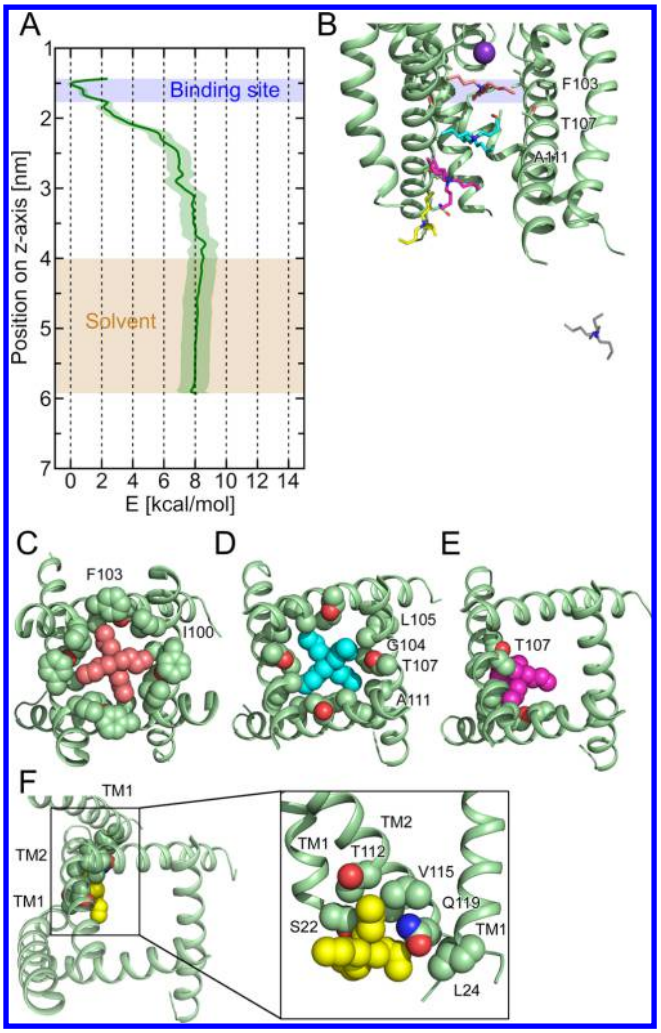

Figure 7. A) Free energy profile of TBA dissociation from the fully open KcsA channel state. The blue and beige shades depict the high affinity binding site and the solvent compartment, respectively. Statistical error is shown as green shade. B) TBA structures, represented as sticks, show the dissociation pathway through the gate. For clarity, only three SUs are shown in green. Interacting amino acids are depicted as green sticks. TBA structures in panels B and C–F correspond to positions 1.5 nm (pink, C), 2.3 nm (cyan, D), 2.9 nm (magenta, E), 3.6 nm (yellow, F), and 5.2 nm on the *z*-axis. C–E) Top view of TBA and interacting amino acids during dissociation. F) Top and side view of TBA and interacting amino acids on TM1 and TM2 helices.

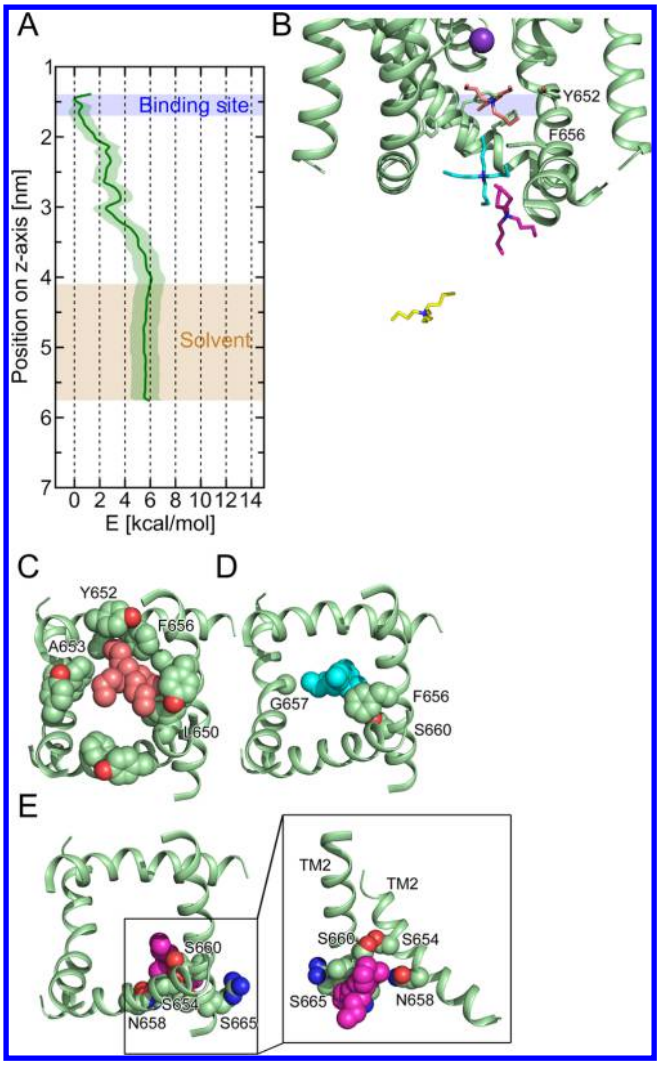

Figure 8. A) Free energy profile of TBA dissociation from the open hERG channel. The blue and beige shades depict the binding site and the solvent compartment, respectively. Statistical error is shown as green shade. B) TBA structures, represented as sticks, show the dissociation pathway through the gate. For clarity, only three SUs are shown in green. The binding determinants Y652 and F656 are depicted as green sticks. TBA structures in panels B and C–E correspond to positions 1.58 nm (pink, C), 2.5 nm (cyan, D), 3 nm (magenta, E), and 4.5 nm (yellow) on the *z*-axis. C–D) Top view of TBA and interacting amino acids during dissociation. E) Top and side view of TBA and interacting amino acids on two adjacent TM2 helices.

TBA shares common features with trapped drugs. Block occurs from the intracellular side of the channel and requires prior channel opening. Further, the drug cannot be washed out during 330 s at resting state and repetitive stimulation during wash-out induces rapid recovery from block, suggesting that TBA is trapped in the hERG cavity (Figure 2E).

In agreement with experimental results, docking and MD simulations support the importance of Y652 and F656 for binding. According to our modeling studies, these interactions are primarily of hydrophobic nature. Cation-pi interactions were not observed; the quaternary nitrogen and aromatic rings of Y652 and F656 were too distant[64] throughout the simulation. This fits to data by Xia et al. showing that higher exposure of the quaternary nitrogen and a decrease of hydrophobicity by shorter alkyl chains leads to reduced potency of QA compounds.[68] Another important component to TBA binding in hERG results from focused helix dipole charges from the pore helices. This is in agreement with a recent study by Dempsey et al.,[75] predicting similar interactions for TBA interactions in KcsA.

The hERG channel closure simulations highlight the important role of F656 during channel closure. Fast transitions of F656 from cavity facing to cavity lining conformation were observed (Figure 4B). This finding is in agreement with a recent MD simulation study revealing innate flexibility of the F656 side chain.[69] Further, it is supported by a mutagenesis study by Fernandez et al.,[16] suggesting an important role of this residue for normal deactivation. Their work cleary showed that replacement of the bulky side chain by smaller hydrophobic amino acids leads to faster channel closure. Therefore, it is

dx.doi.org/10.1021/ci500353r | J. Chem. Inf. Model. 2014, 54, 3218–3228

conceivable that the bulkiness at this position contributes to the slow deactivation kinetics in hERG.

Remarkably, in the presence of TBA, F656 structural rearrangements are significantly perturbed during gating (Figure 4D), indicating that binding of TBA stabilizes the aromatic side chains in the cavity facing conformation. This finding is of particular interest since most hERG blockers bind to F656.[7−10,12−14,18−20] Of note, a study by Chen et al.[76] demonstrated that inactivation leads to gating associated reorientations of Y652 and F656. To what extent the observed conformational changes in our simulation might contribute to inactivation needs to be addressed in future studies.

Interestingly, it has been suggested previously that F656 might act as physical barrier for drug dissociation of certain compounds.[70] It is tempting to speculate that specific interactions with F656 determine if a compound is trapped or not. Based on our simulations, we propose that trapped compounds might stabilize the cavity facing state of F656, presenting a barrier for drug dissociation. Increased sampling of the cavity lining conformation might facilitate drug dissociation prior to complete channel closure. This hypothetical mechanism is illustrated in schematic Figure 9. One way to test the validity of this scenario would be the use of F656 mutants as described by Fernandez et al.,[16] which still exhibit reasonable affinity for blockers while introducing different amino acid size and deactivation kinetics. This approach will be the subject of further studies.

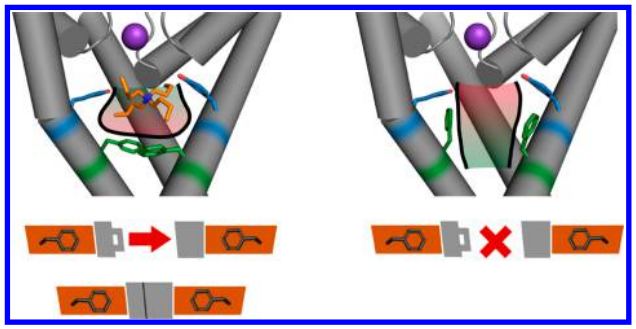

Figure 9. Schematic figure of the importance of the F656 conformation on trapping.

In hERG, not all blockers demonstrate slow recovery from block[23,71,72] but appear to quickly dissociate even when the channels are held at resting state. This might be explained by our findings, demonstrating the important role of F656 during gating. F656 might function as a second gate and prevent dissociation of trapped drugs via mutual interference.

The second important question that was addressed in this study concerns the extent of gate opening necessary for dissociation. Force probe MD simulations and energy calculations on 3 different KcsA crystal structures with pore diameters of up to 14 Å (fully open) revealed that dissociation is only possible when the gate is fully open. Similarly, no energy barrier was found for TBA dissociation from the open hERG state model. In both channels, TBA moves along the cavity wall maximizing hydrophobic contacts to the protein during dissociation. The exit scenario from closed and intermediate KcsA channel states is predicted to trigger conformational changes of TBA to the S_4 conformation. Despite this more compressed structure (diameter of 8 Å), large energy barriers render dissociation from these states highly unlikely. Since except for F103, only small residues line the cavity in KcsA, the observed high energy barriers (40−50 kcal/mol) result primarily from the conformational state, defined by the backbone coordinates. Although high energy barriers occurred during dissociation from these channel states, our force probe simulations did not cause changes in the protein secondary structure. Taken together, we propose that compounds cannot dissociate from closed or intermediate states but require an open helix bundle crossing gate. This is supported by earlier findings from our lab.[73]

■ ASSOCIATED CONTENT

Supporting Information

Distribution of dihedral angles of TBA monitored during closing ED simulations in KcsA and hERG and histograms of the umbrella sampling windows. This material is available free of charge via the Internet at http://pubs.acs.org.

■ AUTHOR INFORMATION

Corresponding Author

*E-mail: anna.stary@univie.ac.at.

Author Contributions

Conceived and designed the experiments: T.L., P.S., E.T., S.H., A.S.W. Performed the experiments: T.L., P.S. Analyzed the data: T.L., P.S., E.T., S.H., A.S.W. Wrote the paper: T.L., P.S., E.T., S.H., A.S.W. All authors have given approval to the final version of the manuscript.

Funding

This work was supported by the Austrian Science Fund (FWF; Grants P22395 and W1232; http://www.fwf.ac.at). Tobias Linder was supported by a research fellowship from the University of Vienna and an EMBO short-term fellowship. Anna Stary-Weinzinger is supported by the Johanna Mahlke, geb. Obermann Stiftung.

Notes

The authors declare no competing financial interest.

■ ACKNOWLEDGMENTS

The computational results presented have been achieved using the Vienna Scientific Cluster (VSC).

■ ABBREVIATIONS

ED, essential dynamics; hERG, human ether-à-go-go related gene; LQTS, long QT syndrome; SF, selectivity filter; TBA, tetrabutylammonium; TEA, tetraethylammonium; QA, quaternary ammonium

■ REFERENCES

(1) Bagal, S. K.; Brown, A. D.; Cox, P. J.; Omoto, K.; Owen, R. M.; Pryde, D. C.; Sidders, B.; Skerratt, S. E.; Stevens, E. B.; Storer, R. I.; Swain, N. A. Ion Channels as Therapeutic Targets: A Drug Discovery Perspective. *J. Med. Chem.* **2013**, *56*, 593−624.

(2) Fermini, B.; Fossa, A. A. The Impact of Drug-Induced QT Interval Prolongation on Drug Discovery and Development. *Nat. Rev. Drug Discovery* **2003**, *2*, 439−447.

(3) Chiang, C. E.; Roden, D. M. The Long QT Syndromes: Genetic Basis and Clinical Implications. *J. Am. Coll. Cardiol.* **2000**, *36*, 1−12.

(4) Keating, M. T.; Sanguinetti, M. C. Molecular and Cellular Mechanisms of Cardiac Arrhythmias. *Cell* **2001**, *104*, 569−580.

(5) Jehle, J.; Schweizer, P. A.; Katus, H. A.; Thomas, D. Novel Roles for hERG K(+) Channels in Cell Proliferation and Apoptosis. *Cell Death Dis.* **2011**, *2*, e193.

(6) Pier, D. M.; Shehatou, G. S.; Giblett, S.; Pullar, C. E.; Tresize, D. J.; Pritchard, C. A.; Challiss, J.; Mitcheson, J. S. Long-Term Channel

Block Is Required to Inhibit Cellular Transformation by Human Ether-a-Go-Go-Related Gene (Herg1) Potassium Channels. *Mol. Pharmacol.* **2014**, *86*, 211−21.
(7) Mitcheson, J. S.; Chen, J.; Lin, M.; Culberson, C.; Sanguinetti, M. C. A Structural Basis for Drug-Induced Long QT Syndrome. *Proc. Natl. Acad. Sci. U. S. A.* **2000**, *97*, 12329−12333.
(8) Lees-Miller, J. P.; Duan, Y.; Teng, G. Q.; Duff, H. J. Molecular Determinant of High-Affinity Dofetilide Binding to HERG1 Expressed in Xenopus Oocytes: Involvement of S6 Sites. *Mol. Pharmacol.* **2000**, *57*, 367−374.
(9) Kamiya, K.; Mitcheson, J. S.; Yasui, K.; Kodama, I.; Sanguinetti, M. C. Open Channel Block of HERG K(+) Channels by Vesnarinone. *Mol. Pharmacol.* **2001**, *60*, 244−253.
(10) Sánchez-Chapula, J. A.; Navarro-Polanco, R. A.; Culberson, C.; Chen, J.; Sanguinetti, M. C. Molecular Determinants of Voltage-Dependent Human Ether-a-Go-Go Related Gene (HERG) K+ Channel Block. *J. Biol. Chem.* **2002**, *277*, 23587−23595.
(11) Sănchez-Chapula, J. A.; Ferrer, T.; Navarro-Polanco, R. A.; Sanguinetti, M. C. Voltage-Dependent Profile of Human Ether-a-Go-Go-Related Gene Channel Block Is Influenced by a Single Residue in the S6 Transmembrane Domain. *Mol. Pharmacol.* **2003**, *63*, 1051−1058.
(12) Sánchez-Chapula, J. A.; Navarro-Polanco, R. A.; Sanguinetti, M. C. Block of Wild-Type and Inactivation-Deficient Human Ether-a-Go-Go-Related Gene K+ Channels by Halofantrine. *Naunyn-Schmiedeberg's Arch. Pharmacol.* **2004**, *370*, 484−491.
(13) Ridley, J. M.; Dooley, P. C.; Milnes, J. T.; Witchel, H. J.; Hancox, J. C. Lidoflazine Is a High Affinity Blocker of the HERG K(+)channel. *J. Mol. Cell. Cardiol.* **2004**, *36*, 701−705.
(14) Perry, M.; de Groot, M. J.; Helliwell, R.; Leishman, D.; Tristani-Firouzi, M.; Sanguinetti, M. C.; Mitcheson, J. Structural Determinants of HERG Channel Block by Clofilium and Ibutilide. *Mol. Pharmacol.* **2004**, *66*, 240−249.
(15) Witchel, H. J.; Dempsey, C. E.; Sessions, R. B.; Perry, M.; Milnes, J. T.; Hancox, J. C.; Mitcheson, J. S. The Low-Potency, Voltage-Dependent HERG Blocker Propafenone - Molecular Determinants and Drug Trapping. *Mol. Pharmacol.* **2004**, *66*, 1201−1212.
(16) Fernandez, D.; Ghanta, A.; Kauffman, G. W.; Sanguinetti, M. C. Physicochemical Features of the HERG Channel Drug Binding Site. *J. Biol. Chem.* **2004**, *279*, 10120−10127.
(17) Sanguinetti, M. C.; Mitcheson, J. S. Predicting Drug-hERG Channel Interactions That Cause Acquired Long QT Syndrome. *Trends Pharmacol. Sci.* **2005**, *26*, 119−124.
(18) Kamiya, K.; Niwa, R.; Mitcheson, J. S.; Sanguinetti, M. C. Molecular Determinants of HERG Channel Block. *Mol. Pharmacol.* **2006**, *69*, 1709−1716.
(19) Guo, J.; Gang, H.; Zhang, S. Molecular Determinants of Cocaine Block of Human Ether-Á-Go-Go-Related Gene Potassium Channels. *J. Pharmacol. Exp. Ther.* **2006**, *317*, 865−874.
(20) Kamiya, K.; Niwa, R.; Morishima, M.; Honjo, H.; Sanguinetti, M. C. Molecular Determinants of hERG Channel Block by Terfenadine and Cisapride. *J. Pharmacol. Sci.* **2008**, *108*, 301−307.
(21) Carmeliet, E. Voltage- and Time-Dependent Block of the Delayed K+ Current in Cardiac Myocytes by Dofetilide. *J. Pharmacol. Exp. Ther.* **1992**, *262*, 809−817.
(22) Mitcheson, J. S.; Chen, J.; Sanguinetti, M. C. Trapping of a Methanesulfonanilide by Closure of the HERG Potassium Channel Activation Gate. *J. Gen. Physiol.* **2000**, *115*, 229−240.
(23) Stork, D.; Timin, E. N.; Berjukow, S.; Huber, C.; Hohaus, A.; Auer, M.; Hering, S. State Dependent Dissociation of HERG Channel Inhibitors. *Br. J. Pharmacol.* **2007**, *151*, 1368−1376.
(24) Windisch, A.; Timin, E.; Schwarz, T.; Stork-Riedler, D.; Erker, T.; Ecker, G.; Hering, S. Trapping and Dissociation of Propafenone Derivatives in HERG Channels. *Br. J. Pharmacol.* **2011**, *162*, 1542−1552.
(25) Di Veroli, G. Y.; Davies, M. R.; Zhang, H.; Abi-Gerges, N.; Boyett, M. R. hERG Inhibitors With Similar Potency But Different Binding Kinetics Do Not Pose the Same Proarrhythmic Risk: Implications for Drug Safety Assessment. *J. Cardiovasc. Electrophysiol.* **2013**, *25*, 197−207.
(26) Armstrong, C. M. Interaction of Tetraethylammonium Ion Derivatives with the Potassium Channels of Giant Axons. *J. Gen. Physiol.* **1971**, *58*, 413−437.
(27) Armstrong, C. M.; Hille, B. The Inner Quaternary Ammonium Ion Receptor in Potassium Channels of the Node of Ranvier. *J. Gen. Physiol.* **1972**, *59*, 388−400.
(28) MacKinnon, R.; Yellen, G. Mutations Affecting TEA Blockade and Ion Permeation in Voltage-Activated K+ Channels. *Science* **1990**, *250*, 276−279.
(29) Luzhkov, V. B.; Aqvist, J. Mechanisms of Tetraethylammonium Ion Block in the KcsA Potassium Channel. *FEBS Lett.* **2001**, *495*, 191−196.
(30) Zhou, M.; Morais-Cabral, J. H.; Mann, S.; MacKinnon, R. Potassium Channel Receptor Site for the Inactivation Gate and Quaternary Amine Inhibitors. *Nature* **2001**, *411*, 657−661.
(31) Holmgren, M.; Smith, P. L.; Yellen, G. Trapping of Organic Blockers by Closing of Voltage-Dependent K+ Channels: Evidence for a Trap Door Mechanism of Activation Gating. *J. Gen. Physiol.* **1997**, *109*, 527−535.
(32) Posson, D. J.; McCoy, J. G.; Nimigean, C. M. The Voltage-Dependent Gate in MthK Potassium Channels Is Located at the Selectivity Filter. *Nat. Struct. Mol. Biol.* **2013**, *20*, 159−166.
(33) Yellen, G.; Jurman, M. E.; Abramson, T.; MacKinnon, R. Mutations Affecting Internal TEA Blockade Identify the Probable Pore-Forming Region of a K+ Channel. *Science (80-.)* **1991**, *251*, 939−942.
(34) Choi, K. L.; Mossman, C.; Aubé, J.; Yellen, G. The Internal Quaternary Ammonium Receptor Site of Shaker Potassium Channels. *Neuron* **1993**, *10*, 533−541.
(35) Crouzy, S.; Bernèche, S.; Roux, B. Extracellular Blockade of K(+) Channels by TEA: Results from Molecular Dynamics Simulations of the KcsA Channel. *J. Gen. Physiol.* **2001**, *118*, 207−218.
(36) Lenaeus, M. J.; Vamvouka, M.; Focia, P. J.; Gross, A. Structural Basis of TEA Blockade in a Model Potassium Channel. *Nat. Struct. Mol. Biol.* **2005**, *12*, 454−459.
(37) Faraldo-Gómez, J. D.; Kutluay, E.; Jogini, V.; Zhao, Y.; Heginbotham, L.; Roux, B. Mechanism of Intracellular Block of the KcsA K+ Channel by Tetrabutylammonium: Insights from X-Ray Crystallography, Electrophysiology and Replica-Exchange Molecular Dynamics Simulations. *J. Mol. Biol.* **2007**, *365*, 649−662.
(38) Yohannan, S.; Hu, Y.; Zhou, Y. Crystallographic Study of the Tetrabutylammonium Block to the KcsA K+ Channel. *J. Mol. Biol.* **2007**, *366*, 806−814.
(39) Cuello, L. G.; Jogini, V.; Cortes, D. M.; Perozo, E. Structural Mechanism of C-Type Inactivation in K(+) Channels. *Nature* **2010**, *466*, 203−208.
(40) Stary, A.; Wacker, S. J.; Boukharta, L.; Zachariae, U.; Karimi-Nejad, Y.; Aqvist, J.; Vriend, G.; de Groot, B. L. Toward a Consensus Model of the HERG Potassium Channel. *ChemMedChem* **2010**, *5*, 455−467.
(41) Wang, J.; Wolf, R. M.; Caldwell, J. W.; Kollman, P. A.; Case, D. A. Development and Testing of a General Amber Force Field. *J. Comput. Chem.* **2004**, *25*, 1157−1174.
(42) Frisch, M. J.; Trucks, G. W.; Schlegel, H. B.; Scuseria, G. E.; Robb, M. A.; Cheeseman, J. R.; Scalmani, G.; Barone, V.; Mennucci, B.; Petersson, G. A.; Nakatsuji, H.; Caricato, M.; Li, X.; Hratchian, H. P.; Izmaylov, A. F.; Bloino, J.; Zheng, G.; Sonnenberg, J. L.; Hada, M.; Ehara, M.; Toyota, K.; Fukuda, R.; Hasegawa, J.; Ishida, M.; Nakajima, T.; Honda, Y.; Kitao, O.; Nakai, H.; Vreven, T.; Montgomery, J. A., Jr.; Peralta, J. E.; Ogliaro, F.; Bearpark, M.; Heyd, J. J.; Brothers, E.; Kudin, K. N.; Staroverov, V. N.; Kobayashi, R.; Normand, J.; Raghavachari, K.; Rendell, A.; Burant, J. C.; Iyengar, S. S.; Tomasi, J.; Cossi, M.; Rega, N.; Millam, J. M.; Klene, M.; Knox, J. E.; Cross, J. B.; Bakken, V.; Adamo, C.; Jaramillo, J.; Gomperts, R.; Stratmann, R. E.; Yazyev, O.; Austin, A. J.; Cammi, R.; Pomelli, C.; Ochterski, J. W.; Martin, R. L.; Morokuma, K.; Zakrzewski, V. G.; Voth, G. A.; Salvador, P.; Dannenberg, J. J.; Dapprich, S.; Daniels, A. D.; Farkas, Ö.;

Foresman, J. B.; Ortiz, J. V.; Cioslowski, J.; Fox, D. J. *Gaussian 09*; 2009.
(43) Wang, J.; Wang, W.; Kollman, P. A.; Case, D. A. Automatic Atom Type and Bond Type Perception in Molecular Mechanical Calculations. *J. Mol. Graphics Modell.* **2006**, *25*, 247−260.
(44) Case, D. A.; Darden, T. A.; Cheatham, T. E.; Simmerling, C. L.; Wang, J.; Duke, R. E.; Luo, R.; Crowley, M.; Walker, R. C.; Zhang, W.; Merz, K. M.; Wang, B.; Hayik, S.; Roitberg, A.; Seabra, G.; Kolossváry, I.; Wong, K. F.; Paesani, F.; Vanicek, J.; Wu, X.; Brozell, S. R.; Steinbrecher, T.; Gohlke, H.; Yang, L.; Tan, C.; Mongan, J.; Hornak, V.; Cui, G.; Mathews, D. H.; Seetin, M. G.; Sagui, C.; Babin, V.; Kollman, P. A. *Amber 11*; 2010.
(45) Wolf, M. G.; Hoefling, M.; Aponte-Santamaría, C.; Grubmüller, H.; Groenhof, G. G_membed: Efficient Insertion of a Membrane Protein into an Equilibrated Lipid Bilayer with Minimal Perturbation. *J. Comput. Chem.* **2010**, *31*, 2169−2174.
(46) Aqvist, J.; Luzhkov, V. Ion Permeation Mechanism of the Potassium Channel. *Nature* **2000**, *404*, 881−884.
(47) Hess, B.; Kutzner, C.; van der Spoel, D.; Lindahl, E. GROMACS 4: Algorithms for Highly Efficient, Load-Balanced, and Scalable Molecular Simulation. *J. Chem. Theory Comput.* **2008**, *4*, 435−447.
(48) Hornak, V.; Abel, R.; Okur, A.; Strockbine, B.; Roitberg, A.; Simmerling, C. Comparison of Multiple Amber Force Fields and Development of Improved Protein Backbone Parameters. *Proteins* **2006**, *65*, 712−725.
(49) Jorgensen, W. L.; Chandrasekhar, J.; Madura, J. D.; Impey, R. W.; Klein, M. L. Comparison of Simple Potential Functions for Simulating Liquid Water. *J. Chem. Phys.* **1983**, *79*, 926.
(50) Berger, O.; Edholm, O.; Jahnig, F. Molecular Dynamics Simulations of a Fluid Bilayer of Dipalmitoylphosphatidylcholine at Full Hydration, Constant Pressure, and Constant Temperature. *Biophys. J.* **1997**, *72*, 2002−2013.
(51) Joung, I. S.; Cheatham, T. E. Determination of Alkali and Halide Monovalent Ion Parameters for Use in Explicitly Solvated Biomolecular Simulations. *J. Phys. Chem. B* **2008**, *112*, 9020−9041.
(52) Darden, T.; York, D.; Pedersen, L. Particle Mesh Ewald: An N log(N) Method for Ewald Sums in Large Systems. *J. Chem. Phys.* **1993**, *98*, 10089.
(53) Hess, B.; Bekker, H.; Berendsen, H. J. C.; Fraaije, J. G. E. M. LINCS: A Linear Constraint Solver for Molecular Simulations. *J. Comput. Chem.* **1997**, *18*, 1463−1472.
(54) Nosé, S. A Unified Formulation of the Constant Temperature Molecular Dynamics Methods. *J. Chem. Phys.* **1984**, *81*, 511.
(55) Hoover, W. Canonical Dynamics: Equilibrium Phase-Space Distributions. *Phys. Rev. A* **1985**, *31*, 1695−1697.
(56) Parrinello, M.; Rahman, A. Polymorphic Transitions in Single Crystals: A New Molecular Dynamics Method. *J. Appl. Phys.* **1981**, *52*, 7182.
(57) Linder, T.; de Groot, B. L.; Stary-Weinzinger, A. Probing the Energy Landscape of Activation Gating of the Bacterial Potassium Channel KcsA. *PLoS Comput. Biol.* **2013**, *9*, e1003058.
(58) Hub, J. S.; de Groot, B. L.; van der Spoel, D. g_wham—A Free Weighted Histogram Analysis Implementation Including Robust Error and Autocorrelation Estimates. *J. Chem. Theory Comput.* **2010**, *6*, 3713−3720.
(59) Sanguinetti, M. C.; Jiang, C.; Curran, M. E.; Keating, M. T. A Mechanistic Link between an Inherited and an Acquird Cardiac Arrthytmia: HERG Encodes the IKr Potassium Channel. *Cell* **1995**, *81*, 299−307.
(60) Baburin, I.; Beyl, S.; Hering, S. Automated Fast Perfusion of Xenopus Oocytes for Drug Screening. *Pflugers Arch.* **2006**, *453*, 117−123.
(61) Luzhkov, V. B.; Österberg, F.; Acharya, P.; Chattopadhyaya, J.; Aqvist, J. Computational and NMR Study of Quaternary Ammonium Ion Conformations in Solution. *Phys. Chem. Chem. Phys.* **2002**, *4*, 4640−4647.
(62) Faraldo-Gómez, J. D.; Roux, B. Characterization of Conformational Equilibria through Hamiltonian and Temperature Replica-Exchange Simulations: Assessing Entropic and Environmental Effects. *J. Comput. Chem.* **2007**, *28*, 1634−1647.
(63) Choi, K.-H.; Song, C.; Shin, D.; Park, S. hERG Channel Blockade by Externally Applied Quaternary Ammonium Derivatives. *Biochim. Biophys. Acta* **2011**, *1808*, 1560−1566.
(64) Marshall, M. S.; Steele, R. P.; Thanthiriwatte, K. S.; Sherrill, C. D. Potential Energy Curves for Cation-Pi Interactions: Off-Axis Configurations Are Also Attractive. *J. Phys. Chem. A* **2009**, *113*, 13628−13632.
(65) Zhou, Y.; Morais-Cabral, J. H.; Kaufman, A.; MacKinnon, R. Chemistry of Ion Coordination and Hydration Revealed by a K+ Channel-Fab Complex at 2.0 A Resolution. *Nature* **2001**, *414*, 43−48.
(66) Perrin, M. J.; Kuchel, P. W.; Campbell, T. J.; Vandenberg, J. I. Drug Binding to the Inactivated State Is Necessary but Not Sufficient for High-Affinity Binding to Human Ether-À-Go-Go-Related Gene Channels. *Mol. Pharmacol.* **2008**, *74*, 1443−1452.
(67) Hill, A. P.; Perrin, M. J.; Heide, J.; Campbell, T. J.; Mann, S. A; Vandenberg, J. I. Kinetics of Drug Interaction with the Kv11.1 Potassium Channel. *Mol. Pharmacol.* **2014**, *85*, 769−776.
(68) Xia, M.; Shahane, S. A.; Huang, R.; Titus, S. A.; Shum, E.; Zhao, Y.; Southall, N.; Zheng, W.; Witt, K. L.; Tice, R. R.; Austin, C. P. Identification of Quaternary Ammonium Compounds as Potent Inhibitors of hERG Potassium Channels. *Toxicol. Appl. Pharmacol.* **2011**, *252*, 250−258.
(69) Knape, K.; Linder, T.; Wolschann, P.; Beyer, A.; Stary-Weinzinger, A. In Silico Analysis of Conformational Changes Induced by Mutation of Aromatic Binding Residues: Consequences for Drug Binding in the hERG K+ Channel. *PLoS One* **2011**, *6*, e28778.
(70) Karczewski, J.; Wang, J.; Kane, S. A.; Kiss, L.; Koblan, K. S.; Culberson, J. C.; Spencer, R. H. Analogs of MK-499 Are Differentially Affected by a Mutation in the S6 Domain of the hERG K+ Channel. *Biochem. Pharmacol.* **2009**, *77*, 1602−1611.
(71) Milnes, J. T.; Crociani, O.; Arcangeli, A.; Hancox, J. C.; Witchel, H. J. Blockade of HERG Potassium Currents by Fluvoxamine: Incomplete Attenuation by S6Mutations at F656 or Y652. *Br. J. Pharmacol.* **2003**, *139*, 887−898.
(72) Mitcheson, J. S. hERG Potassium Channels and the Structural Basis of Drug-Induced Arrhythmias. *Chem. Res. Toxicol.* **2008**, *21*, 1005−1010.
(73) Beyl, S.; Timin, E. N.; Hohaus, A.; Stary, A.; Kudrnac, M.; Guy, R. H.; Hering, S. Probing the Architecture of an L-Type Calcium Channel with a Charged Phenylalkylamine: Evidence for a Widely Open Pore and Drug Trapping. *J. Biol. Chem.* **2007**, *282*, 3864−3870.
(74) Imai, Y. N.; Ryu, S.; Oiki, S. Docking Model of Drug Binding to the Human Ether-à-go-go Potassium Channel Gudied by Tandem Dimer Mutant Patch-Clamp Data: A Synergic Approach. *J. Med. Chem.* **2009**, *52*, 1630−1638.
(75) Dempsey, C. E.; Wright, D.; Colenso, C. K.; Sessions, R. B.; Hancox, J. C. Assessing hERG Pore Models As Templates for Drug Docking Using Published Experimental Constraints: The Inactivated State in the Context of Drug Block. *J. Chem. Inf. Model.* **2014**, *54*, 601−612.
(76) Chen, J.; Seebohm, G.; Sanguinetti, M. C. Position of aromatic residues in the S6 dfomain, not inactivation, dictates cisapride sensitivity of HERG and eag potassium channels. *Proc. Natl. Acad. Sci. U. S. A.* **2002**, *99*, 12461−12466.